Development of elastodynamic finite integration technique for two-dimensional micropolar elastodynamics

Takahiro SAITOH[1)], Yusuke SUZUKI[2)], Taizo MARUYAMA[3)], Akira FURUKAWA[4)], Sohichi HIROSE[5)], Davinder KUMAR[6)], Dilbag SINGH[7)] and S. K. TOMAR[8)]

1)Gunma University (1-5-1, Kiryu, Tenjin, Gunma, 376-8515, Japan, E-mail:t-saitoh@gunma-u.ac.jp)
2)Gunma University (1-5-1, Kiryu, Tenjin, Gunma, 376-8515, Japan, E-mail:t160c050@gunma-u.ac.jp)
3)Ehime University (3, Bunkyo, Matsuyama, Ehime, 790-8577, Japan, E-mail:maruyama@cee.ehime-u.ac.jp)
4)Hokkaido University (Kita 13, Nishsi 8, Kita-ku, Sapporo, Hokkaido, 060-8628, Japan, E-mail:afurukawa@eng.hokudai.ac.jp)
5)Tokyo Institute of Technology (2-12-1, O-okayama, Meguro, Tokyo, 152-8552, Japan, E-mail:shirose@cv.titech.ac.jp)
6)Panjab University (Chandigarh - 160 014, India, E-mail:davinderkgoriwal@gmail.com)
7)Panjab University (Chandigarh - 160 014, India, E-mail:kahlondilbag80@gmail.com)
8)Panjab University (Chandigarh - 160 014, India, E-mail:sktomar@pu.ac.in)

This study presents a micropolar elastodynamic finite integration technique (M-EFIT) formulation for two-dimensional (2-D) micropolar elastodynamics. In general, the classical theory of elasticity deals with homogeneous elastic solids and does not take microscopic inhomogeneity into account. Therefore, numerical methods based on the classical theory of elasticity cannot be used to accurately simulate wave propagation behaviors in micropolar materials, owing to their microscopic inhomogeneity. In this research, we focus on the micropolar elastodynamic theory. According to the micropolar theory, three kinds of waves with different wave velocities exist in micropolar elastic solids, of which two have dispersibility in a 2-D formulation. In this study, an EFIT is proposed for 2-D micropolar elastodynamics. Numerical examples of wave propagation, reflection, and transmission in 2-D micropolar elastodynamics are demonstrated to validate the proposed M-EFIT formulation.

Key Words: Elastodynamic Finite Integration Technique (EFIT), Micropolar elastodynamics, Wave propagation, Reflection and Transmission

1. Introduction

This study presents a micropolar elastodynamic finite integration technique (M-EFIT) formulation for two-dimensional (2-D) micropolar elastodynamics. Understanding elastic wave propagation is important in the fields of ultrasonic nondestructive testing (UT) and seismic engineering. Therefore, many types of numerical techniques[(1)(2)] for wave analysis have been developed and used in several engineering fields. In general, the classical theory of elasticity deals with homogeneous elastic solids and does not take microscopic inhomogeneity into account[(3)]. However, it has been established that an unexplained wave propagation phenomenon occurs under the assumption of such a linear elastic theory. For example, the famous one of such problems has been advocated by Biot[(4)]. In general, only one kind of P-wave exists in homogeneous isotropic solids. Nevertheless, Biot proved the existence of two types of P-waves in fluid-saturated porous solids. In addition, Eringen[(5)] integrated the effect of microscopic inhomogeneity into the linear elasticity theory, extending the linear elasticity theory[(6)]. This extended linear elastodynamic theory, which considers the effect of microscopie inhomogenity, is called the micropolar elastodynamic theory. Concretes, bedrocks, and human bones are examples of typical micropolar materials. According to the micropolar elastodynamic theory, three kinds of waves (P-, S-, and M-waves) with different wave velocities exist in micropolar elastic solids, of which two (S- and M-waves) have dispersibility in 2-D in-plane problems. However, many simulations for elastic wave propagation in such micropolar materials use the conventional linear elastodynamic theory rather than the micropolar elastodynamic theory because the micropolar elastodynamic theory and its application to numerical methods are very complex. Therefore, it is significant to develop a wave propagation simulation tool based on the micropolar elastodynamic the-

Received Sep. 2, 2021, accepted Nov. 6. 2021

ory.

The finite difference time-domain method (FDTD)[7][8] is probably the easiest way to develop such a simulation tool. However, the drawback of the FDTD method is obscure boundary conditions. To improve the drawback of the FDTD method, an EFIT[9] was developed. Schubert[10] solved linear and nonlinear elastodynamic problems using the EFIT. Nakahata et al.[11] analyzed wave propagation in austenitic steel with anisotropy using EFIT. Their simulations are valuable, but all the formulations are based on the classical elastodynamic theory, and no numerical examples obtained by EFIT for wave problems considering the micropolar elastodynamic theory are known to our knowledge.

Therefore, in this research, a micropolar EFIT (which is called M-EFIT) is developed for wave propagation in micropolar elastodynamics. In the following sections, a brief description of the micropolar elastodynamic theory and the EFIT formulation are described. Time and space discretization and how to handle boundary conditions are discussed. Following the demonstration of some numerical examples obtained using 2-D M-EFIT, our future research plan is presented.

2. Micropolar elastodynamic theory

A brief description of the micropolar elastodynamic theory is presented in this section. Unless otherwise stated, subscripts are used throughout this paper, such as $(\ )_i$, where i equals 1 or 3. In addition, summation over repeated subscripts is implied throughout this paper. The equations of motion, the strain-displacement relations, and the constitutive relations for 2-D linear isotropic micropolar elastic solids can be written, respectively, as follows:

$$\sigma_{ji,j} + \rho b_i = \rho \ddot{u}_i \tag{1}$$

$$\epsilon_{ij} = u_{j,i} - e_{2ij}\phi_2 \tag{2}$$

$$\sigma_{ij} = \lambda \epsilon_{kk}\delta_{ij} + (\mu + \kappa)\epsilon_{ij} + \mu \epsilon_{ji} \tag{3}$$

where u_i and ϕ_i represent displacement and microrotation, respectively. In addition, b_i is the body force, ϵ_{ij} is the strain, σ_{ij} is the stress, δ_{ij} is the Kronecker delta, e_{ijk} is the alternating tensor, and ρ is the density. $\dot{(\ )}$ and $(\ )_{,i}$ indicate the partial derivative with respect to time t and space x_i, respectively. In the micropolar elastodynamic theory, the microrotation ϕ_i, the couple stress m_{ij}, and the microrotation strain ψ_{ij} must be considered. Their basic equations can be written as follows:

$$m_{i2,i} + e_{2ij}\sigma_{ij} + l_2 = \rho J \ddot{\phi}_2 \tag{4}$$

$$\psi_{i2} = \phi_{2,i} \tag{5}$$

$$m_{i2} = \gamma \psi_{i2} \tag{6}$$

where l_i represents the body couple and J represents the microinertia. Note that unlike in the case of the classical elastodynamic theory, the stress σ_{ij} and strain ϵ_{ij} are not symmetric. In Eqs.(3) and (6), λ, μ, κ, and γ represent micropolar elastic constants and

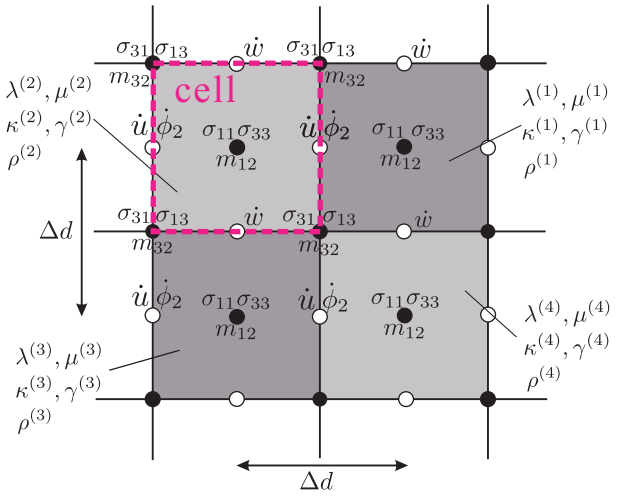

Fig. 1 Definition of a finite volume V with boundary S.

they can be rewritten by the corresponding physically easier interpretation constants[12] as follows:

$$G = \frac{2\mu + \kappa}{2} \tag{7}$$

$$\nu = \frac{\lambda}{2\lambda + 2\mu + \kappa} \tag{8}$$

$$L = \sqrt{\frac{\gamma(\mu + \kappa)}{\kappa(2\mu + \kappa)}} \tag{9}$$

$$N = \sqrt{\frac{\kappa}{2(\mu + \kappa)}} \tag{10}$$

In Eqs.(7) and (8), G and ν represent the shear modulus and Poisson ratio, respectively. The parameter L in Eq.(9) denotes the microstructure length of a material. In addition, the non-dimensionless parameter N in Eq.(10) shows the strength of a micropolar property. The parameter β is introduced using the Poisson ratio in Eq.(8) as follow:

$$\beta = \frac{1 - 2\nu}{2(1 - \nu)} \tag{11}$$

This parameter β is related to $c_L = c_T/\beta$, where c_L represents the P-wave velocity, which does not depend on frequency. In addition, c_T is given by $c_T = \sqrt{G/\rho}$. Eqs.(1) - (6) are discretized for time and space according to the EFIT scheme. More details of the micropolar elastodynamics can be seen in the reference [13].

3. M-EFIT formulation

3.1. Integrations over the cell

In this M-EFIT formulation, Eqs.(1) - (6) are not directly discretized. In the EFIT, an analysis domain is represented with the grid and then, the grid is divided into cells, as shown in Fig. 1. Assuming that the body force b_i and the body couple l_i are equal to

zero and considering Gauss's divergence theorem, equations of motion (1) for the stress and (4) for the couple stress are first integrated with the surface S of a cell for a finite volume V, as follows:

$$\int_V \rho \ddot{u}_i dV = \int_S \sigma_{ji} n_j dS \tag{12}$$

$$\int_V \rho J \ddot{\phi}_2 dV = \int_S m_{i2} n_i dS + \int_V e_{2ij} \sigma_{ij} dV \tag{13}$$

where n_i shows the unit outward normal vector for the boundary S. For the constitutive relations (3) and (6), the same integration approach and time derivative are considered, respectively, as follows:

$$\int_V \dot{\sigma}_{ij} dV = \int_S [\lambda \dot{u}_k n_k \delta_{ij} + (\mu + \kappa) \dot{u}_j n_i + \mu \dot{u}_i n_j] dS$$
$$- \int_V [(\mu + \kappa) e_{2ij} \dot{\phi}_2 + \mu e_{2ji} \dot{\phi}_2] dV \tag{14}$$

$$\int_V \dot{m}_{i2} dV = \gamma \int_S \dot{\phi}_2 n_i dS \tag{15}$$

Substituting the subscripts of Eqs.(12) and (13) into 1 or 3 according to the summation convention, the following three equations are obtained as :

$$\int_V \rho \ddot{u} dV = \int_S (\sigma_{11} n_1 + \sigma_{31} n_3) dS \tag{16}$$

$$\int_V \rho \ddot{w} dV = \int_S (\sigma_{13} n_1 + \sigma_{33} n_3) dS \tag{17}$$

$$\int_V \rho J \ddot{\phi}_2 dV = \int_S (m_{12} n_1 + m_{32} n_3) dS + \int_V (\sigma_{31} - \sigma_{13}) dV \tag{18}$$

where explicit engineering expressions are used, as shown by $u_1 = u$ and $u_3 = w^{(8)(11)}$, for simplicity. In addition, the constitutive relations (14) and (15) can be rewritten in the same manner, as follows:

$$\int_V \dot{\sigma}_{11} dV = \int_S [(2\mu + \kappa + \lambda) \dot{u} n_1 + \lambda \dot{w} n_3] dS \tag{19}$$

$$\int_V \dot{\sigma}_{33} dV = \int_S [\lambda \dot{u} n_1 + (2\mu + \kappa + \lambda) \dot{w} n_3] dS \tag{20}$$

$$\int_V \dot{\sigma}_{31} dV = \int_S [(\mu + \kappa) \dot{u} n_3 + \mu \dot{w} n_1] dS - \int_v \kappa \dot{\phi}_2 dV \tag{21}$$

$$\int_V \dot{\sigma}_{13} dV = \int_S [(\mu + \kappa) \dot{w} n_1 + \mu \dot{u} n_3] dS + \int_v \kappa \dot{\phi}_2 dV \tag{22}$$

$$\int_V \dot{m}_{12} dV = \gamma \int_S \dot{\phi}_2 n_1 dS \tag{23}$$

$$\int_V \dot{m}_{32} dV = \gamma \int_S \dot{\phi}_2 n_3 dS \tag{24}$$

For Eqs.(16) - (24), spatial and time discretization are considered.

3.2. Spatial discretization for M-EFIT

In this M-EFIT formulation, Eqs. (16) - (24) must be discretized for space and time. As previously mentioned, the EFIT requires integration over the square cell V with the surface S, as defined in Fig. 1. For each cell, the normal stresses σ_{11} and σ_{33} and the couple stress m_{12} are represented by the values at the center of the cell, as shown in Fig. 1. At that time, the particle velocities $\dot{u}$ and $\dot{w}$, and the microrotational velocities $\dot{\phi}_2$ are arranged at the midpoints of the edges, as shown in Fig. 1. On the other hand, the shear stresses

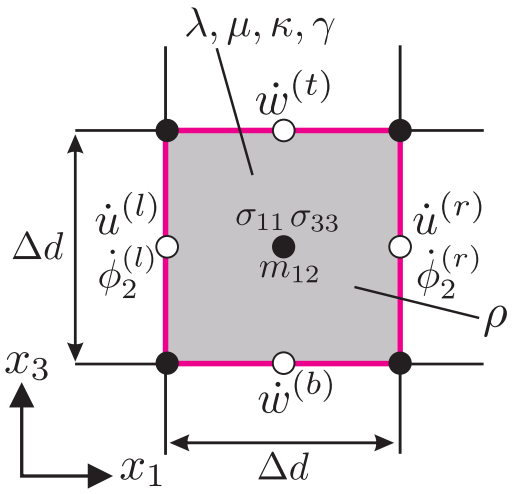

Fig. 2 Spatial discretization of σ_{11}, σ_{33} and m_{12} for M-EFIT.

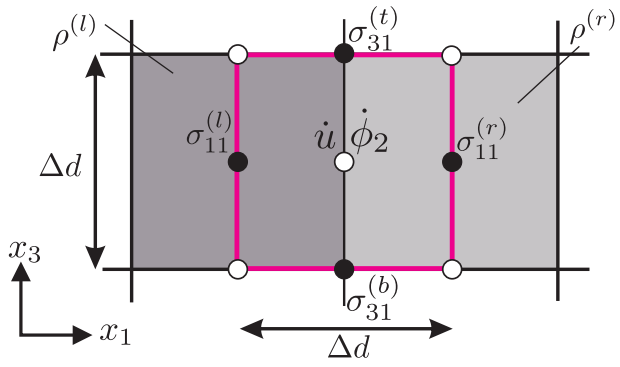

Fig. 3 Spatial discretization of $\dot{u}$ and $\dot{\phi}_2$ for M-EFIT.

σ_{31} and σ_{13} and the couple stress m_{32} are arranged at the corner of the cell. Therefore, considering a cell enclosed by the red solid square of the integral volume V as shown in Fig. 2, Eqs.(19), (20) and (23) can be discretized for space, respectively, as follow:

$$\dot{\sigma}_{11} \simeq \frac{1}{\Delta d} \left[(2\mu + \kappa + \lambda) \left(\dot{u}^{(r)} - \dot{u}^{(l)} \right) + \lambda \left(\dot{w}^{(t)} - \dot{w}^{(b)} \right) \right] \tag{25}$$

$$\dot{\sigma}_{33} \simeq \frac{1}{\Delta d} \left[\lambda \left(\dot{u}^{(r)} - \dot{u}^{(l)} \right) + (2\mu + \kappa + \lambda) \left(\dot{w}^{(t)} - \dot{w}^{(b)} \right) \right] \tag{26}$$

$$\dot{m}_{12} \simeq \frac{\gamma}{\Delta d} \left[\dot{\phi}_2^{(r)} - \dot{\phi}_2^{(l)} \right] \tag{27}$$

where Δd is the length of the integral volume V and the superscripts (r), (l), (t), and (b) express the position of the physical quantity seen from the center of the cell. Similarly, Eqs.(16) and (18) are discretized for space using the integral volume enclosed by the red square in Fig. 3, as follows:

$$\ddot{u} \simeq \frac{1}{\bar{\rho}} \frac{1}{\Delta d} \left(\sigma_{11}^{(r)} - \sigma_{11}^{(l)} + \sigma_{31}^{(t)} - \sigma_{31}^{(b)} \right) \tag{28}$$

$$\ddot{\phi}_2 \simeq \frac{1}{\bar{\rho} J} \frac{1}{\Delta d} \left(m_{12}^{(r)} - m_{12}^{(l)} + m_{32}^{(t)} - m_{32}^{(b)} \right)$$
$$+ \frac{1}{2} \left(\sigma_{31}^{(t)} + \sigma_{31}^{(b)} \right) - \frac{1}{2} \left(\sigma_{13}^{(t)} + \sigma_{13}^{(b)} \right) \tag{29}$$

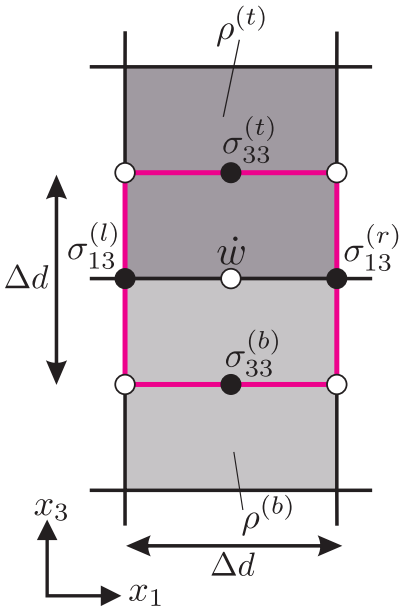

Fig.4 Spatial discretization of w for M-EFIT.

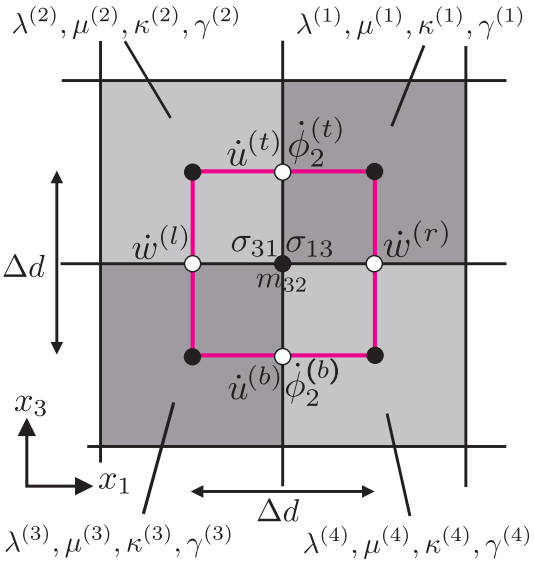

Fig.5 Spatial discretization of σ_{31}, σ_{13} and m_{32} for M-EFIT.

In Eqs.(28) and (29), $\bar{\rho}$ is the average density of right and left cells, as shown in Fig. 3, which is given by

$$\bar{\rho} = \frac{1}{2}(\rho^{(r)} + \rho^{(l)}) \tag{30}$$

where $\rho^{(r)}$ and $\rho^{(l)}$ are the densities of the right and left cells, respectively. Moreover, the spatial discretization for Eq.(17) is calculated by considering the node allocation of Fig. 4 as follows:

$$\ddot{w} \simeq \frac{1}{\bar{\rho}} \frac{1}{\Delta d} \left(\sigma_{13}^{(r)} - \sigma_{13}^{(l)} + \sigma_{33}^{(t)} - \sigma_{33}^{(b)} \right). \tag{31}$$

Finally, Eqs.(21), (22) and (24) are discretized according to the red square cell in Fig.5, respectively, as follows:

$$\dot{\sigma}_{31} \simeq \frac{1}{\Delta d} \left[(\mu + \kappa) \left(\dot{u}^{(t)} - \dot{u}^{(b)} \right) + \mu \left(\dot{w}^{(r)} - \dot{w}^{(l)} \right) \right] - \frac{\kappa}{2} \left(\dot{\phi}_2^{(t)} + \dot{\phi}_2^{(b)} \right) \tag{32}$$

$$\dot{\sigma}_{13} \simeq \frac{1}{\Delta d} \left[(\mu + \kappa) \left(\dot{w}^{(r)} - \dot{w}^{(l)} \right) + \mu \left(\dot{u}^{(t)} - \dot{u}^{(b)} \right) \right] + \frac{\kappa}{2} \left(\dot{\phi}_2^{(t)} + \dot{\phi}_2^{(b)} \right) \tag{33}$$

$$\dot{m}_{32} \simeq \frac{\gamma}{\Delta d} \left[\dot{\phi}_2^{(t)} - \dot{\phi}_2^{(b)} \right] \tag{34}$$

The left-hand sides of Eqs. (25) - (34) include the time derivative. This time derivative is computed using the standard time integration, as described in the following section.

3.3. Time discretization for M-EFIT

In the time-domain, the stress component $\boldsymbol{\sigma}$ and couple stress component $\boldsymbol{m}$ are allocated at half-time steps, whereas the particle velocities $\dot{\boldsymbol{u}}$ and $\dot{\boldsymbol{w}}$ and the microrotational velocity $\dot{\boldsymbol{\phi}}$ are allocated at full-time steps. Therefore, the following time discretization yields an explicit leap-frog scheme:

$$\{\boldsymbol{\sigma}\}^{n+\frac{1}{2}} \simeq \{\boldsymbol{\sigma}\}^{n-\frac{1}{2}} + \Delta t \{\dot{\boldsymbol{\sigma}}\}^{n} \tag{35}$$

$$\{\boldsymbol{m}\}^{n+\frac{1}{2}} \simeq \{\boldsymbol{m}\}^{n-\frac{1}{2}} + \Delta t \{\dot{\boldsymbol{m}}\}^{n} \tag{36}$$

$$\{\dot{\boldsymbol{u}}\}^{n+1} \simeq \{\dot{\boldsymbol{u}}\}^{n} + \Delta t \{\ddot{\boldsymbol{u}}\}^{n+\frac{1}{2}} \tag{37}$$

$$\{\dot{\boldsymbol{w}}\}^{n+1} \simeq \{\dot{\boldsymbol{w}}\}^{n} + \Delta t \{\ddot{\boldsymbol{w}}\}^{n+\frac{1}{2}} \tag{38}$$

$$\{\dot{\boldsymbol{\phi}}\}^{n+1} \simeq \{\dot{\boldsymbol{\phi}}\}^{n} + \Delta t \{\ddot{\boldsymbol{\phi}}\}^{n+\frac{1}{2}} \tag{39}$$

where Δt represents the time interval and the superscript n denotes multiple integers of a time step of Δt. Nine physical quantities, σ_{11}, σ_{33}, σ_{13}, σ_{31}, $\dot{u}$, $\dot{w}$, $\dot{m}_{12}$, $\dot{m}_{32}$, and $\dot{\phi}_2$ at each node can be obtained by solving Eqs. (35) - (39) with initial and boundary conditions. In general, the treatment of boundary surfaces in the EFIT is unique[9] compared to that in FDTD[8]. The treatment of boundary surfaces in the EFIT is discussed in the next section.

3.4. Treatment of boundary surface

The EFIT is a grid-based numerical method based on the finite differential equation and can easily and explicitly treat the boundary conditions on the interface between different materials. A brief description of how to deal with the free reflection boundaries in the EFIT is discussed in this section. The traction $\boldsymbol{t}$ and the couple $\boldsymbol{m}$ must be zero in the free reflection boundaries, as shown in Fig. 6. Therefore, the following equations are satisfied:

$$t_i = n_j \sigma_{ji} = 0, \quad m_2 = n_i m_{i2} = 0 \tag{40}$$

The traction $\boldsymbol{t}$ and couple $\boldsymbol{m}$ of Eq. (40) can be rewritten on the free reflection boundary in Fig. 6 as follows:

$$t_1 = n_1 \sigma_{11} + n_3 \sigma_{31} = 0 \tag{41}$$

$$t_3 = n_1 \sigma_{13} + n_3 \sigma_{33} = 0 \tag{42}$$

$$m_2 = n_1 m_{12} + n_3 m_{32} = 0 \tag{43}$$

Therefore, as shown in Fig. 6, the shear stress σ_{31} allocated to the free reflection boundary between air and a solid must be zero. For this case, the shear stress σ_{13} and the couple stress m_{32} are also located on the same node for the shear stress σ_{31}, as shown in Fig. 1. In such a situation, however, the normal stresses, σ_{11} and σ_{33}, and the couple stress m_{12} cannot be allocated to the nodes of the free reflection boundaries as well as σ_{31}, σ_{13}, and m_{32}. Therefore, it is necessary to implement a particular handling method for meeting the free reflection boundary conditions for the normal stresses, $\sigma_{11} = 0$ and $\sigma_{33} = 0$, and the couple stress, $m_{12} = 0$.

In Fig. 6, the outward unit normal vector components n_1 and n_3 are given by $n_1 = -1$ and $n_3 = 0$, respectively. Now, the stresses σ_{11} and σ_{13} and the couple stress m_{12} must be zero in order to satisfy Eqs. (41)-(43). Here, a virtual node is considered to satisfy the normal stress $\sigma_{11} = 0$ on the free reflection boundary in Fig. 6. Considering the normal stress $\sigma_{11}^{(l)}$ on the virtual node whose color is red, as shown in Fig. 6, the following equation on the free reflection boundary is derived:

$$\frac{1}{2}(\sigma_{11}^{(r)} + \sigma_{11}^{(l)}) = 0 \tag{44}$$

To satisfy Eq. (44) on the free reflection boundary in Fig. 6, Eq. (44) is substituted into Eq. (28) to yield the following equation:

$$\ddot{u} \simeq \frac{1}{\bar{\rho}} \frac{1}{\Delta d} \left(2\sigma_{11}^{(r)}\right) \tag{45}$$

The same approach used for the normal stress σ_{11} is considered for the normal stress σ_{33} and the couple m_{12}, which are located on the same node. Therefore, the normal stress σ_{33} and the couple m_{12} satisfy the equations, respectively, as follows:

$$\frac{1}{2}(\sigma_{33}^{(r)} + \sigma_{33}^{(l)}) = 0 \tag{46}$$

$$\frac{1}{2}(m_{12}^{(r)} + m_{12}^{(l)}) = 0 \tag{47}$$

This treatment can be applied to the boundary between the base metal and the cavity with traction free.

In general, only the grid and node are considered in the FDTD method. Therefore, the material parameters must be defined on the grid nodes. However, in the EFIT, the material parameters are defined for each cell. Consequently, the physical quantities on the boundary between multiple cells are calculated by averaging the material constants of each cell, as shown in Figs. 3, 4, and 5 because the EFIT formulation starts with the integral of the governing equations. Since such averaging process cannot be handled by the FDTD method, the EFIT is easier to deal with boundary conditions than the FDTD method, as shown in this section.

4. Numerical examples

Some numerical examples are shown in this section. In the following numerical examples, the density ρ and the micro-inertia J of micropolar elastic solids are set as $\rho = 4.5$ and $J = 0.175$, respectively. In addition, the micropolar elastic constants λ, μ, κ, and γ are equal to $\lambda = 1.5$, $\mu = 1.0$, $\kappa = 1.0$, and $\gamma = 0.375$,

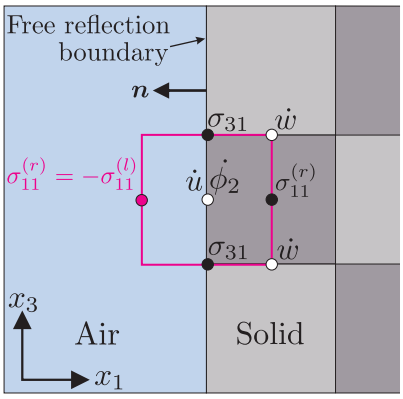

Fig. 6 The treatment on a virtual node in the vicinity of the free reflection boundary.

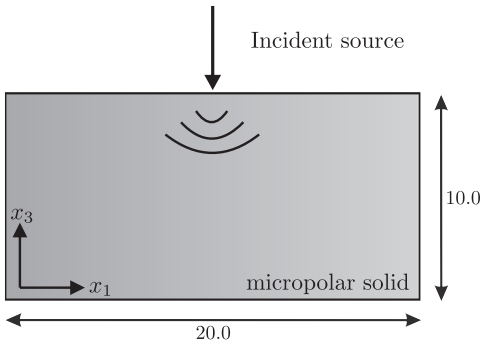

Fig.7 Analysis model for elastic wave propagation in a micropolar elastic solid.

respectively. Therefore, the parameter β is calculated as $\beta = 1/3$ using Eq. (11). These parameters were determined according to the paper by Fukui et al.[12]. In this case, the phase velocity of P-wave is given by $c_L = 1.0$. The grid size Δd and the time step size Δt are equal to $\Delta d = 5.0 \times 10^{-3}$ and $\Delta t = 2.5 \times 10^{-4}$, respectively. The incident source is given as the following boundary condition at the center of the top surface of the micropolar material:

$$\dot{w}^{\text{in}}(t) = \sin\left(\frac{2\pi t}{T}\right) H(T - t) \tag{48}$$

where T represents the period of the incident source, which is given by $T = 1.0$. In addition, the function H denotes the step function. In addition, $\dot{u} = \dot{w} = \dot{\phi}_2 = 0$ in the analysis domain are considered as the initial conditions. The workstation with the Intel(R) Xeon(R) W-2235 CPU @ 3.80GHz and 64 GB memory is used for the following computations.

4.1. Elastic wave propagation in a micropolar elastic solid

As a first numerical example, the elastic wave propagation in a micropolar elastic solid, as shown in Fig. 7, is analyzed using the proposed M-EFIT. The width w_l and height h_l of this model are $w_l = 20$ and $h_l = 10$, respectively. The traction free boundary condition is given at the surfaces, except for the center of the top surface, where the incident source defined in Eq. (48) is considered. The elastic wave propagation behavior in a micropolar elastic

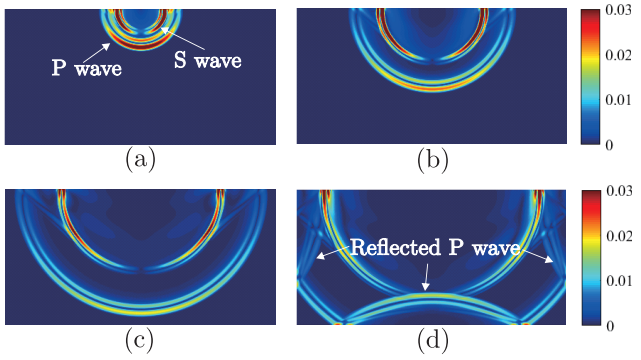

Fig. 8 P- and S-wave propagation in the micropolar elastic solid in Fig. 7 at times (a) $t = 12500\Delta t$ (b) $25000\Delta t$ (c) $37500\Delta t$ and (d) $50000\Delta t$.

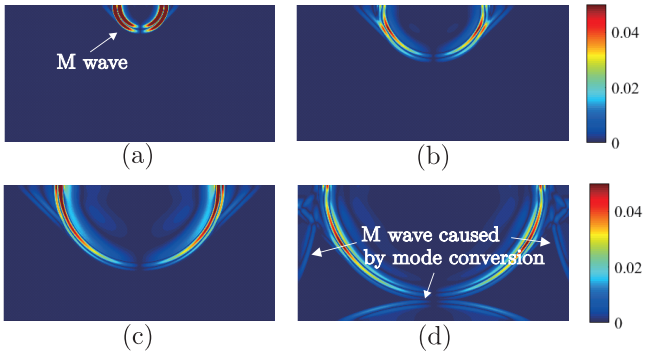

Fig. 9 M-wave propagation in the micropolar elastic solid in Fig. 7 at times (a) $t = 12500\Delta t$ (b) $25000\Delta t$ (c) $37500\Delta t$ and (d) $50000\Delta t$.

solid is confirmed by solving this problem.

Fig. 8 shows the absolute value of the particle velocity, $\sqrt{\dot{u}^2 + \dot{w}^2}$, in the analysis model in Fig. 7 at times $t = 12500\Delta t$, $25000\Delta t$, $37500\Delta t$, and $50000\Delta t$. As shown in Fig. 8(a), P- and S-waves are excited by the incident source given by Eq. (48). The absolute values of particle velocities for S-wave directly below the incident source are small compared with those for P-wave because the incident source is given in the x_3 direction, as shown in Figs. 8(a) and (b). In addition, the reflected P-waves generated by the right, left, and bottom surfaces can be seen in Fig. 8(d).

Fig. 9 demonstrates the absolute value of the particle velocity of the microrotation $\dot{\phi}_2$ in a micropolar elastic solid, as shown in Fig. 7. As shown in Figs. 9(a), (b), and (c), M-wave excitation and propagation can be confirmed. Moreover, in Fig. 9(d), the reflected M-waves from the right, left, and bottom surfaces can be seen before the incident M-wave excited by Eq. (48) arrives at these surfaces. This is because the mode conversion of P-wave reflection, as shown in Fig. 8, at each surface occurs. In general, the explicit M-wave velocity cannot obtain in the time-domain. However, velocities of M-wave are almost the same as those of S-wave at several frequencies in the frequency-domain[12]. Therefore, it is expected that the M-wave speed is approximately equal to S-wave one in the time-domain. Indeed, we can see that the M-wave speed is almost the same as S-wave one from Figs. 8 and 9. The required computational time and memory are about 5 hours and 1133MB, respectively.

4.2. Elastic wave propagation in a bimaterial of micropolar and isotropic solids

Next, the analysis of elastic waves in a bimaterial composed of the micropolar solid and an isotropic solid is performed. In this analysis, the density ρ and the micro-inertia J of an isotropic material are given by $\rho = 4.5$ and $J = 0.0$, respectively. In addition, the isotropic material part in Fig. 10 is modeled by providing λ, μ, κ, and γ as $\lambda = 1.5$, $\mu = 1.0$, $\kappa = 0.0$, and $\gamma = 0.0$, respectively. When $\gamma = 0.0$ and $\kappa = 0.0$, Eqs. (9) for L and (10) for N are

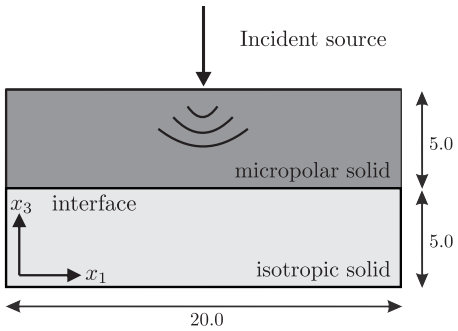

Fig. 10 Analysis model for elastic wave propagation in a bimaterial of a micropolar and an isotropic elastic solid.

zero. As mentioned in Section 2, the parameter L indicates the representative length for microstructure and N shows the micropolar property. Therefore, the isotropic solid can be considered in the M-EFIT formulation by considering the micropolar elastic constants $\gamma = 0.0$ and $\kappa = 0.0$. The width w_l and height h_l of each solid are given by $w = 20.0$ and $h = 5.0$, respectively. The other parameters and the incident source are the same as those used in the previous analysis.

Fig. 11 shows the absolute value of the particle velocity, $\sqrt{\dot{u}^2 + \dot{w}^2}$, in the analysis model in Fig. 10. In each inset figure of Fig. 11, the horizontal solid line drawn in the center indicates the interface between the micropolar and isotropic solid, and the material interface is perfectly connected. As shown in Figs. 11(a) and (b), P- and S-waves are excited by the incident source defined in Eq. (48). The wave fronts of P- and S-waves are distorted by the interface, as shown in Figs. 11(c) and (d). In addition, the head wave by S-wave propagation can be confirmed in Figs. 11(c) and (d). Furthermore, the reflected P-wave by the bottom interface of the isotropic solid and the reflected S-wave by the bimaterial interface are observed.

Fig. 12 shows the absolute value of the particle velocity of the microrotation $\dot{\phi}_2$ in the bimaterial, as shown in Fig. 7. As shown in Figs. 12(a) and (b), M-wave is excited because of the incident source defined in Eq. (48). Then, M-wave is reflected by the bi-

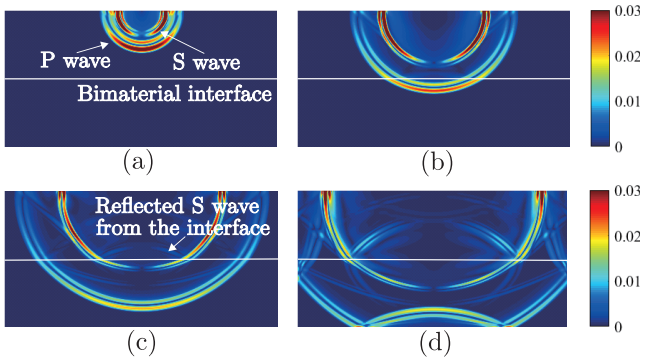

Fig. 11 P- and S-wave propagation in the micropolar elastic solid in Fig. 7 at times (a)$t = 12500\Delta t$ (b)$25000\Delta t$ (c)$37500\Delta t$ and (d)$50000\Delta t$.

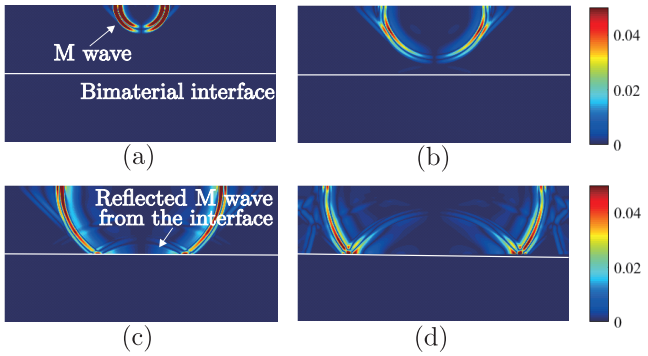

Fig. 12 M-wave propagation in the micropolar elastic solid in Fig. 7 at times (a)$t = 12500\Delta t$ (b)$25000\Delta t$ (c)$37500\Delta t$ and (d)$50000\Delta t$.

material interface, as shown in Fig. 12(c). However, M-wave does not propagate in the isotropic solid. This is because M-wave cannot exist in isotropic materials. The required computational time and memory are about 6 hours and 1133MB, respectively.

These two numerical results confirmed that the P-, S- and M-waves, propagate in micropolar elastic solids correctly, albeit qualitatively.

5. Conclusion

In this paper, M-EFIT for 2-D elastic wave propagation in micropolar elastic solids was proposed. The formulation of the proposed M-EFIT herein is based on the micropolar elastodynamic theory derived by Eringen[5][6]. The validity of the proposed M-EFIT was confirmed by simulating P-, S- and M-wave propagation in 2-D micropolar elastic solids. As seen in the classical elastodynamic theory, it can be confirmed that M-wave cannot exist in the isotropic solid side of the bimaterial. In addition, M-wave can be generated by the mode conversion of P- and S-waves. The proposed M-EFIT is an explicit method and can solve large-scale problems within a relatively shorter time than other numerical methods. However, the proposed M-EFIT cannot handle infinite regions without any modifications. Therefore, in future work, the PML(Perfectly Matched Layer)[14] for the proposed formulation will be developed to handle an infinite micropolar elastodynamic domain. In addition, a convolution quadrature-based time-domain boundary element method (CQBEM)[15][16] that can treat infinite regions will be developed for 2-D micropolar elastodynamics. More complex wave propagation in a micropolar material will be analyzed using the proposed M-EFIT by referencing some mathematical formulas about micropolar elastodynamic problems[17]. Also, this work presented in the paper will be extended to 3-D problems.

Acknowledgment

This work was supported by "Joint Usage/Research Center for Interdisciplinary Large-scale Information Infrastructures" and "High Performance Computing Infrastructure" in Japan (Project ID:jh200052-NAH and jh210033-NAH), the bilateral exchange research between Japan and India (JPJSBP1 20207707 and DST/INT/JSPS/P-322/2020), and "JSPS KAKENHI (21K0423100)".

References

(1) Kobayashi, S. et al.: *Wave analysis and boundary element method*, (2000), Kyoto University Press (in Japanese).

(2) Seriani, G. and Oliveira, S. P.: Numerical modeling of mechanical wave propagation, *La Rivista del Nuovo Cimento*, **43** (2020), pp. 459-514.

(3) Eringen, A.C. and Suhubi, E.S.: Elastodynamics: Vol.1 and 2, (1975), Academic Press Inc.

(4) Biot, M. A.: Theory of propagation of elastic waves in a fluid-saturated porous solid, I. Low-frequency range, *J. Acoust. Soc. Am.*, **28** (1956), pp. 168-178.

(5) Eringen, A. C.: Linear theory of micropolar elasticity, *J. Math. Mech.*, **15** (1966), pp. 909-923.

(6) Eringen, A. C.: Microcontinuum Field Theories-I. Foundations and Solids, (1999), Springer, New York.

(7) Yu, W., Yang, X., Liu, Y., Mittra, R. and Muto, A.: Advanced FDTD method: Parallelization, acceleration, and engineering applications, (2011), Artech House.

(8) Satoh, M.: Introduction to analysis of elastic vibration and wave by FDTD method, (2015), Corona Publishing (in Japanese).

(9) Fellinger, P., Marklein, R., Langenberg, K. J. and Klaholz, S.: Numerical modeling of elastic wave propagation and scattering with EFIT -elastodynamic finite integration technique-, *Wave motion*, **21**(1) (1995), pp.47-66.

(10) Schubert, F.: Numerical time-domain modeling of linear and nonlinear ultrasonic wave propagation using finite integration techniques - Theory and applications, Fast verification of solutions of matrix equations, *Ultrasonics*, **42** (2004), pp.221-229.

(11) Nakahata, K., Hirose, S., Schubert, F. and Köhler, B.: Image based EFIT simulation for nondestructive ultrasonic testing of austenitic steel, *J. Solid. Mech. Mat. Eng.*,**3**(12), (2009), 1256-1262.

(12) Fukui, T. and Okui, Y.: Boundary element analysis of scattering problems in two dimensional micropolar elasticity, In; Boundary element methods -Current Research in Japan and China-, M. Tanaka, Q. Du and T. Honma (eds.), (1993), pp. 283-292.

(13) Nowacki, W.: Theory of asymmetric elasticity, (1986), PWN-Polish Scientific Pub.

(14) Givoli, D.: High-order local non-reflecting boundary conditions: a review, *Wave Motion*, Vol.39,(2004), pp.319-326.

(15) Saitoh, T., Hirose, S. and Fukui, T. : Convolution quadrature boundary element method and acceleration by fast multipole method in 2-D viscoelastic wave propagation, *Theor. and Appl. Mech. Japan*, **57**(2009), pp. 385-393.

(16) Furukawa, A., Saitoh, T. and Hirose, S.: Convolution quadrature time-domain boundary element method for 2-D and 3-D elastodynamic analyses in general anisotropic elastic solids, *Eng. Anal. Bound. Elem.*, **39**(2014), pp.64-74.

(17) Kaliraman, V, Poonia, R. K.: Elastic wave propagation at imperfect boundary of micropolar elastic solid and fluid saturated porous solid half-space, *J. Solid Mech.*, **10**(3) (2018), pp.655-671.